ACS APPLIED MATERIALS & INTERFACES

Research Article

www.acsami.org

Star-Shaped D−A Small Molecules Based on Diketopyrrolopyrrole and Triphenylamine for Efficient Solution-Processed Organic Solar Cells

Jun-Ying Pan, Li-Jian Zuo, Xiao-Lian Hu, Wei-Fei Fu, Mei-Rong Chen, Lei Fu, Xiao Gu, Hang-Qi Shi, Min-Min Shi,* Han-Ying Li, and Hong-Zheng Chen

State Key Laboratory of Silicon Materials, MOE Key Laboratory of Macromolecular Synthesis and Functionalization, & Department of Polymer Science and Engineering, Zhejiang University, Hangzhou 310027, P. R. China

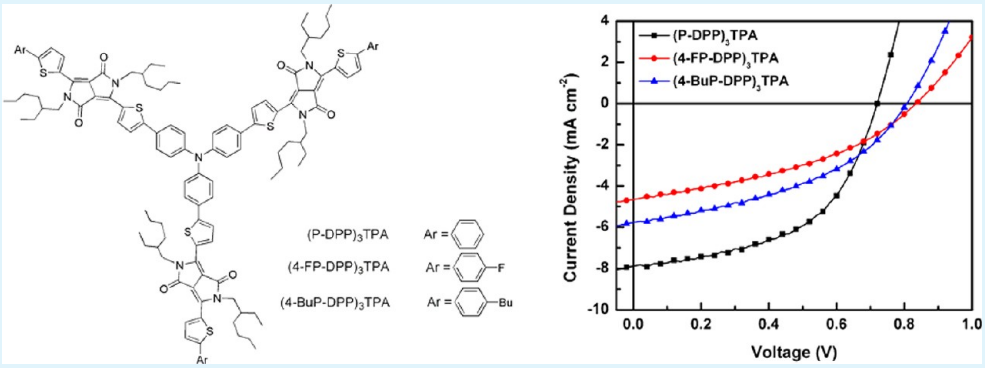

ABSTRACT: Three star-shaped D−A small molecules, $(P\text{-}DPP)_3TPA$, $(4\text{-}FP\text{-}DPP)_3TPA$, and $(4\text{-}BuP\text{-}DPP)_3TPA$ were designed and synthesized with triphenylamine (TPA) as the core, diketopyrrolopyrrole (DPP) as the arm, and unsubstituted or substituted benzene rings (phenyl, P; 4-fluoro-phenyl, 4-FP; 4-*n*-butyl-phenyl, 4-BuP) as the end-group. All the three small molecules show relatively narrow optical band gaps (1.68−1.72 eV) and low-lying highest occupied molecular orbital (HOMO) energy levels (−5.09∼−5.13 eV), implying that they are potentially good electron donors for organic solar cells (OSCs). Then, photovoltaic properties of the small molecules blended with [6,6]-phenyl-C_{61}-butyric acid methyl ester ($PC_{61}BM$) as electron acceptor were investigated. Among three small molecules, the OSC based on $(P\text{-}DPP)_3TPA$:PCBM blend exhibits a best power conversion efficiency (PCE) of 2.98% with an open-circuit voltage (V_{oc}) of 0.72 V, a short-circuit current density (J_{sc}) of 7.94 mA/cm^2, and a fill factor (*FF*) of 52.2%, which may be ascribed to the highest hole mobility of $(P\text{-}DPP)_3TPA$.

KEYWORDS: *small molecule, organic solar cells, star-shaped, diketopyrrolopyrrole, triphenylamine*

INTRODUCTION

Organic solar cells (OSCs) have become a promising alternative strategy to relieve the global energy crisis due to their advantages of low-cost (solution processing), lightweight, flexible substrates, and so on.[1−3] OSCs typically consist of an active-layer having a phase-separated blend of an electron donor and an electron acceptor (bulk-heterojunction, BHJ) placed between a tin-doped indium oxide (ITO) anode and a low work function metal cathode.[3] Ideal donor materials should have the following two key characteristics: One is the narrow band gap (E_g) (to increase the short-circuit current density J_{sc} of the device) and the other is the deep HOMO (highest occupied molecular orbital) energy level (to increase the open-circuit voltage V_{oc}).[4] Nowadays, donor−acceptor (D−A, push−pull) molecular structure has become the most efficient strategy used in the design and synthesis of donor materials. Low band gap donors can be obtained through using this push−pull approach.[5−8] To date, the highest power conversion efficiency (PCE) reported has reached 9.2% by using low band gap polymers in BHJ-structured OSCs,[9] and the OSCs based on small molecules have also yielded a PCE as high as 7.38%.[10]

Although PCEs of small-molecule BHJ solar cells are still lower than their polymeric counterparts, they have recently attracted considerable attention due to their advantages of well-defined structure, easier purification, less batch-to-batch variation in properties, and intrinsic monodispersity.[2,11,12] Therefore, it is believed that small molecule BHJ solar cells are promising to realize their commercial application in the future.

As a well-known electron-donating moiety, triphenylamine (TPA) has been widely used to design D−A polymers and small molecules for the applications in OSCs. In recent years, many TPA-based star-shaped and linear small molecules for OSCs have been reported, and most of them showed good photovoltaic performances.[13−15] For example, Zhan and co-workers reported a D−A−D small molecule with TPA as the core, benzothiadiazole as the arm, and oligothiophene as the end-group. The resulting OSC provided a PCE of 4.3%.[16] They also synthesized a linear A-D-D organic small molecule

Received: November 8, 2012
Accepted: January 15, 2013
Published: January 15, 2013

Scheme 1. Synthetic Route to Three Star-Shaped D-A Small Molecules

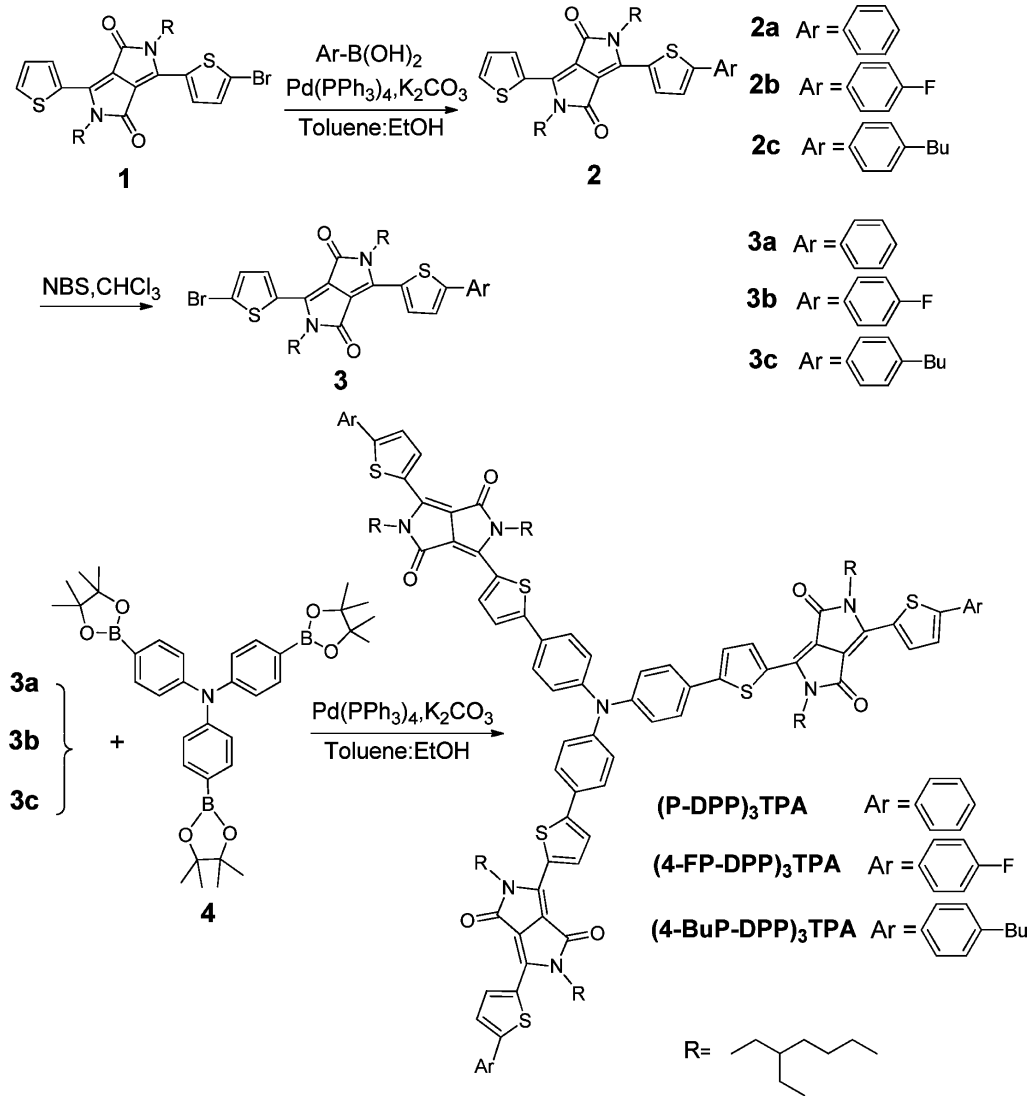

TT-TTPA with thiazolothiazole (TT) as acceptor unit, thiophene (T) as bridge, and TPA as the donor unit. The OSC based on the blend of TT-TTPA and [6,6]-phenyl-C_{71}-butyric acid methyl ester ($PC_{71}BM$) afforded a PCE of 3.73%.[17] Many studies have shown that the star-shaped molecules exhibit deeper HOMO energy levels, better solution-processability, higher isotropy in light absorption and charge transportation, compared to the corresponding linear molecules. Meanwhile, increasing the number of electron-withdrawing groups in TPA-based D−A molecules was demonstrated to be an effective approach to deepen the HOMO energy level, to narrow the band gap, and to consequently increase the V_{oc} and J_{sc} in the device.[18]

Diketopyrrolopyrrole (DPP) unit is promising for solar cell applications because of its advantages of strong light absorption, photochemical stability, and large-scale synthesis.[19−22] As a strong electron-withdrawing moiety, DPP has been coupled with a variety of electron-rich groups to provide low band gap polymers and small molecules for BHJ solar cells.[23−26] For example, a series of low-band gap DPP-based polymers have been reported by Huo et al, and the OSCs based on these polymers showed the best PCE of 4.45%.[23] And it is also reported that BHJ solar cells based on a small molecule with DPP as the core and benzofuran as the terminating group yielded a PCE as high as 4.4%.[24]

With the above considerations in mind, the combination of TPA and DPP units is expected to provide promising low band gap molecules due to the strong intramolecular D−A interaction. Besides, the energy levels and aggregation state of the starburst molecules can be fine-tuned by introducing different end-groups onto the DPP moiety.[27] And the phenyl group is chosen as the end-group because it can offer good stability for the target small molecules.[28−31] Therefore, in this paper, three star-shaped D−A small molecules, $(P\text{-}DPP)_3TPA$, $(4\text{-}FP\text{-}DPP)_3TPA$ and $(4\text{-}BuP\text{-}DPP)_3TPA$, where TPA is used as the core, DPP as the arm, and unsubstituted or substituted benzene rings (phenyl, P; 4-fluoro-phenyl, 4-FP; 4-*n*-butyl-phenyl, 4-BuP) as the end-group, were designed and synthesized. The thermal stability, optical absorption, and HOMO energy levels of the obtained small molecules were fully characterized. Preliminary photovoltaic study of small molecule:[6,6]-phenyl-C_{61}-butyric acid methyl ester ($PC_{61}BM$) blends were conducted and a good PCE up to 2.98% could be achieved.

dx.doi.org/10.1021/am302623k | ACS Appl. Mater. Interfaces 2013, 5, 972−980

EXPERIMENTAL SECTION

Instrument. ^{1}H NMR spectra were obtained on a Bruker DMX-300 nuclear magnetic resonance spectroscope. UV−visible absorption spectra were recorded on a Shimadzu UV-2450 spectrophotometer. Elemental analyses were carried out on a LECO 932 CHNS elemental analyzer. Thermogravimetric analysis (TGA) was carried out on a WCT-2 thermal balance under protection of nitrogen at a heating rate of 20 °C/min. Cyclic voltammetry (CV) was done on a CHI 660C electrochemical workstation with Pt disk, Pt plate, and standard calomel electrode (SCE) as working electrode, counter electrode, and reference electrode, respectively, in a 0.1 mol/L tetrabutylammonium hexafluorophosphate (Bu_4NPF_6) CH_2Cl_2 solution. Topographic images of the films were obtained on a Veeco MultiMode atomic force microscopy (AFM) in the tapping mode using an etched silicon cantilever at a nominal load of ∼2 nN, and the scanning rate for a 5 μm × 5 μm image size was 1.0 Hz.

Materials. All reagents, unless otherwise specified, were obtained from Aldrich, Acros, and TCI Chemical Co. and used as received. All the solvents were freshly distilled prior to use. 2,5-Bis(2-ethylhexyl)-3-(5-bromothiophen-2-yl)-6-(thiophen-2-yl)pyrrolo[3,4-c]pyrrole-1,4-(2H,5H)-dione (**1**) and tris-[4-(4,4,5,5-tetramethyl-[1,3,2]-dioxaborolan-2-yl)-phenyl]-amine (**4**) were synthesized according to the reported procedures.[26]

Device Fabrication and Characterization. OSCs were fabricated with indium tin oxide (ITO) glass as the anode, Al as the cathode, and a blended film of donor:$PC_{61}BM$ between the two electrodes as the photoactive layer. The ITO glass was precleaned and PEDOT:PSS [poly(3,4-ethylenedioxythiophene):poly(styrenesulfonate)] (Baytron P 4083, Germany) was spin-coated on the ITO substrate. The thickness of the PEDOT:PSS layer was about 30 nm. Then, a 20 mg/mL solution of $PC_{61}BM$ and donor molecules in different solvents was spin-cast at different speed for 30 s onto the PEDOT:PSS layer. The solvents include chlorobenzene (CB), chloroform (CF), and CF containing 2% 1,8-diiodooctane (DIO). The thickness of the photoactive layer is 120 ± 20 nm (calibrated by an Ambios Technology XP-2 profilometer). At last, a 100 nm thick Al film was deposited on the photoactive layer under vacuum of ∼4 × 10^{-4} Pa. The active area of OSCs is 9 mm^2. Current density−voltage (J−V) characteristics of the devices in the dark and under illumination were recorded on a Keithley 2400-SCS semiconductor parameter analyzer in air. A Thermal Oriel solar simulator was used to give AM 1.5G irradiance of 100 mW/cm^2. External quantum efficiency (EQE) spectra were measured using a Stanford 8300 lock-in amplifier unit coupled with a WDG3 monochromator and a 500 W xenon lamp.

The charge carrier mobility of the blends was measured using the space-charge-limited current (SCLC) method. Hole-only devices were fabricated in a structure of ITO/PEDOT:PSS/donor:$PC_{61}BM$/MoO_3(10 nm)/Al(100 nm). The device characteristics were extracted by modeling the dark current under forward bias using the SCLC expression described by the Mott-Gurney law

$$J = \frac{9}{8}\varepsilon_r\varepsilon_0\mu\frac{V^2}{L^3} \quad (1)$$

Here, $\varepsilon_r \approx 3$ is the average dielectric constant of the blended film, ε_0 is the permittivity of the free space, μ is the carrier mobility, $L \approx 70$ nm is the thickness of the film, and V is the applied voltage.

Synthesis. The general synthetic routes toward small molecules are outlined in Scheme 1. The detailed synthetic processes are as follows.

*2,5-Bis-(2-ethyl-hexyl)-3-(5-phenyl-thiophen-2-yl)-6-thiophen-2-yl-2,5-dihydro-pyrrolo[3,4-c]pyrrole-1,4-dione (**2a**).* Compound **1** (2.5 g, 4.14 mmol), benzeneboronic acid (0.79 g, 6.48 mmol), 2.0 M aqueous K_2CO_3 solution (21.5 mL), ethanol (5 mL), and toluene (80 mL) were mixed together in a 250 mL two-neck flask and purged with nitrogen for 20 min. To this solution was added tetrakis(triphenylphosphine)palladium ($Pd(PPh_3)_4$) (0.17 g), and the reaction mixture was heated at 80 °C under reflux for 36 h. The mixture was extracted in CH_2Cl_2, washed with brine and dried over anhydrous $MgSO_4$, then the solvent was evaporated under vacuum. The crude product was purified by chromatography on silica gel (eluent: CH_2Cl_2/petroleum ether, 2:1, v/v) to provide a purple solid (2.4 g, 96.4%). ^{1}H NMR (300 MHz, $CDCl_3$), δ (ppm): 8.98 (d, 1H), 8.91 (d, 1H), 7.70−7.67 (m, 2H), 7.63−7.60 (m, 1H), 7.48−7.27 (m, 5H), 4.08−4.02 (m, 4H), 1.97−1.83 (m, 2H), 1.42−1.23 (m, 16H), 0.93−0.83 (m, 12H). ^{13}C NMR (300 MHz, $CDCl_3$), δ (ppm): 162.01, 161.85, 150.00, 140.54, 140.16, 137.16, 135.42, 133.35, 130.64, 130.12, 129.40, 129.07, 128.95, 128.65, 126.35, 124.69, 53.70, 46.12, 39.45, 39.30, 30.55, 30.41, 28.79, 28.57, 23.88, 23.73, 23.35, 14.74, 14.02, 10.80, 10.73.

*2,5-Bis-(2-ethyl-hexyl)-3-[5-(4-fluoro-phenyl)-thiophen-2-yl]-6-thiophen-2-yl-2,5-dihydro-pyrrolo[3,4-c]pyrrole-1,4-dione (**2b**).* This compound was prepared by the same procedure as described for compound **2a** with 1 and 1.5 mol equiv of compound **1** and 4-fluorobenzeneboronic acid, respectively, to yield a purple solid (94.0%). ^{1}H NMR (300 MHz, $CDCl_3$), δ (ppm): 8.92 (d, 1H), 8.90 (d, 1H), 7.67−7.62 (m, 3H), 7.40 (d, 1H), 7.29 (d, 1H), 7.16−7.10 (m, 2H), 4.07−4.02 (m, 4H), 1.96−1.82 (m, 2H), 1.41−1.25 (m, 16H), 0.93−0.84 (m, 12H). ^{13}C NMR (300 MHz, $CDCl_3$), δ (ppm): 164.88, 161.94, 161.83, 161.57, 148.69, 140.30, 140.27, 137.11, 135.58, 130.80, 130.06, 129.67, 129.63, 128.94, 128.69, 128.16, 128.05, 124.63, 116.63, 108.17, 53.73, 46.07, 39.42, 39.27, 30.49, 30.37, 29.97, 28.76, 28.54, 23.83, 23.68, 23.38, 23.35, 14.39, 14.35, 10.79, 10.72.

*2,5-Bis-(2-ethyl-hexyl)-3-[5-(4-n-butyl-phenyl)-thiophen-2-yl]-6-thiophen-2-yl-2,5-dihydro-pyrrolo[3,4-c]pyrrole-1,4-dione (**2c**).* This compound was prepared by the same procedure as described for compound **2a** with 1 and 1.5 mol equiv of compound **1** and 4-*n*-butylbenzeneboronic acid, respectively, to yield a purple solid (95.3%). ^{1}H NMR (300 MHz, $CDCl_3$), δ (ppm): 8.97 (d, 1H), 8.86 (d, 1H), 7.62−7.57 (m, 3H), 7.43 (d, 1H), 7.28−7.25 (m, 1H), 7.22 (d, 2H), 4.08−4.02 (m, 4H), 2,65 (t, 2H), 1.98−1.82 (m, 2H), 1.68−1.58 (m, 2H), 1.42−1.24 (m, 18H), 0.97−0.83 (m, 15H). ^{13}C NMR (300 MHz, $CDCl_3$), δ (ppm): 162.06, 161.38, 150.45, 144.35, 140.77, 139.89, 137.33, 135.25, 130.81, 130.33, 130.18, 129.43, 128.60, 128.44, 126.27, 124.22, 108.37, 108.00, 46.12, 39.45, 39.32, 35.66, 33.68, 30.57, 30.46, 29.93, 28.79, 28.60, 23.91, 23.79, 23.34, 23.30, 22.56, 14.30, 14.25, 14.16, 10.79, 10.74.

*2,5-Bis-(2-ethyl-hexyl)-3-(5-bromo-thiophen-2-yl)-6-(5-phenyl-thiophen-2-yl)-2,5-dihydro-pyrrolo[3,4-c]pyrrole-1,4-dione (**3a**).* *N*-bromosuccinimide (NBS) (0.85 g, 4.79 mmol) was added dropwise to a solution of **2a** (2.4 g, 3.99 mmol) in $CHCl_3$ (120 mL) in a one-necked flask at room temperature. The mixture was stirred for an additional 4 h, and then the solvent was removed under reduced pressure. The residue was purified by chromatography on silica gel (eluent: CH_2Cl_2/petroleum ether, 2:1, v/v) to yield a purple solid (2.25 g, 79.5%). ^{1}H NMR (300 MHz, $CDCl_3$), δ (ppm): 8.97 (d, 1H), 8.63 (d, 1H), 7.69 (d, 2H), 7.48−7.34 (m, 4H), 7.21 (d, 1H), 4.08−3.94 (m, 4H), 1.96−1.82 (m, 2H), 1.41−1.22 (m, 16H), 0.93−0.84 (m, 12H). ^{13}C NMR (300 MHz, $CDCl_3$), δ (ppm): 161.88, 161.55, 150.36, 140.96, 138.51, 137.53, 135.29, 133.27, 131.57, 131.52, 129.36, 129.16, 128.83, 126.35, 124.74, 118.74, 108.45, 107.96, 53.71, 46.16, 39.42, 39.31, 30.51, 30.35, 28.76, 28.53, 23.85, 23.74, 23.38, 23.31, 14.37, 14.33, 10.78, 10.72.

*2,5-Bis-(2-ethyl-hexyl)-3-(5-bromo-thiophen-2-yl)-6-[5-(4-fluoro-phenyl)-thiophen-2-yl]-2,5-dihydro-pyrrolo[3,4-c]pyrrole-1,4-dione (**3b**).* This compound was prepared by the same procedure as described for compound **3a** with 1 and 1.2 mol equiv of compound **2b** and NBS, respectively, to yield a purple solid (76.4%). ^{1}H NMR (300 MHz, $CDCl_3$), δ (ppm): 8.92 (d, 1H), 8.64 (d, 1H), 7.66−7.61 (m, 2H), 7.40 (d, 1H), 7.23 (d, 1H), 7.16−7.10 (m, 2H), 4.12−3.88 (m, 4H), 1.95−1.80 (m, 2H), 1.42−1.11 (m, 16H), 0.96−0.77 (m, 12H). ^{13}C NMR (300 MHz, $CDCl_3$), δ (ppm): 164.92, 161.79, 161.50, 149.02, 140.70, 138.73, 137.41, 135.38, 131.60, 131.47, 129.60, 129.56, 128.84, 128.16, 128.05, 124.65, 118.86, 116.66, 116.36, 108.34, 107.97, 53.73, 46.13, 39.39, 39.28, 30.49, 30.33, 28.75, 28.50, 23.83, 23.71, 23.37, 23.32, 14.38, 14.34, 10.78, 10.71.

*2,5-Bis-(2-ethyl-hexyl)-3-(5-bromo-thiophen-2-yl)-6-[5-(4-n-butyl-phenyl)-thiophen-2-yl]-2,5-dihydro-pyrrolo-[3,4-c]pyrrole-1,4-dione (**3c**).* This compound was prepared by the same procedure as described for compound **3a** with 1 and 1.2 mol equiv of compound **2c** and NBS, respectively, to yield a purple solid (77.4%). ^{1}H NMR (300 MHz, $CDCl_3$), δ (ppm): 8.98 (d, 1H), 8.61 (d, 1H), 7.60 (d, 2H), 7.43

(d, 1H), 7.27−7.20 (m, 3H), 4.10−3.94 (m, 4H), 2.65 (t, 2H), 1.96−1.83 (m, 2H), 1.68−1.58 (m, 2H), 1.41−1.24 (m, 18H), 0.97−0.84 (m, 15H). ^{13}C NMR (300 MHz, $CDCl_3$), δ (ppm): 161.90, 161.48, 150.82, 144.47, 141.15, 138.34, 137.78, 135.17, 131.57, 130.69, 129.46, 128.28, 126.26, 124.27, 118.57, 108.47, 107.73, 53.72, 46.15, 39.41, 39.31, 35.70, 33.74, 30.51, 30.35, 29.98, 28.76, 28.53, 23.83, 23.73, 23.39, 23.32, 22.60, 14.38, 14.34, 14.24, 10.78, 10.73.

(P-DPP)$_3$TPA. Compound **3a** (0.83 g, 1.22 mmol), **4** (0.18 g, 0.29 mmol), 2.0 M aqueous K_2CO_3 solution (5.7 mL), ethanol (5 mL), and toluene (70 mL) were mixed together in a 250 mL two-neck flask and purged with nitrogen for 20 min. To this solution was added tetrakis(triphenylphosphine)palladium (0.03 g) and the reaction mixture was heated at 80 °C under reflux for 48 h. The mixture was extracted in CH_2Cl_2, washed with brine, and dried over anhydrous $MgSO_4$, then the solvent was evaporated under vacuum. The crude product was purified by chromatography on silica gel (eluent gradient: CH_2Cl_2/petroleum ether, 2:1−6:1, v/v) to provide a dark blue powder (0.37 g, 62.7%). ^{1}H NMR (300 MHz, $CDCl_3$), δ (ppm): 8.93 (br, 3H), 8.89 (br, 3H), 7.59 (d, 6H), 7.54 (d, 6H), 7.37 (t, 6H), 7.34 (d, 6H), 7.28 (t, 3H), 7.12 (d, 6H), 4.04−3.95 (m, 12H), 1.99−1.87 (m, 6H), 1.36−1.18 (m, 48H), 0.86−0.78 (m, 36H). ^{13}C NMR (300 MHz, $CDCl_3$) δ (ppm): 161.75, 147.20, 139.90, 137.31, 133.40, 129.35, 128.98, 128.72, 127.41, 126.29, 124.82, 124.19, 108.37, 46.22, 39.50, 30.61, 29.94, 28.78, 23.95, 23.36, 14.33, 10.86. Anal. Calcd for $C_{126}H_{141}N_7O_6S_6$: C, 74.11; H, 6.96; N, 4.80. Found: C, 74.11; H, 7.31; N, 4.65.

(4-FP-DPP)$_3$TPA. This compound was prepared by the same procedure as described for compound (P-DPP)$_3$TPA with 4 and 1 mol equiv of compound **3b** and **4**, respectively, to yield a dark blue powder (yield =65.2%). ^{1}H NMR (300 MHz, $CDCl_3$), δ (ppm): 8.97 (br, 3H), 8.87 (br, 3H), 7.68−7.55 (m, 12H), 7.39 (d, 6H), 7.20−7.10 (m, 12H), 4.13−4.00 (m, 12H), 1.98−1.88 (m, 6H), 1.45−1.25 (m, 48H), 0.94−0.85 (m, 36H). ^{13}C NMR (300 MHz, $CDCl_3$) δ (ppm): 164.86, 161.82, 161.75, 161.55, 149.27, 148.39, 147.21, 140.02, 139.58, 137.37, 136.89, 129.73, 129.69, 129.12, 128.70, 128.62, 128.07, 127.96, 127.40, 124.81, 124.56, 124.18, 116.57, 116.28, 108.42, 108.24, 46.21, 39.49, 30.60, 28.82, 28.77, 23.95, 23.35, 14.32, 10.85. Anal. Calcd for $C_{126}H_{138}F_3N_7O_6S_6$: C, 72.21; H, 6.64; N, 4.68. Found: C, 72.06; H, 6.77; N, 4.70.

(4-BuP-DPP)$_3$TPA. This compound was prepared, using 4:1 mol equiv of compound **3c** and **4**, and in the same procedure as was described for (P-DPP)$_3$TPA, to yield a dark blue powder (yield =70.1%). ^{1}H NMR (300 MHz, $CDCl_3$), δ (ppm): 8.99 (br, 3H), 8.96 (br, 3H), 7.60 (t, 12H), 7.43 (d, 6H), 7.25−7.19 (m, 12H), 4.13−4.02 (m, 12H), 2.65 (t, 6H), 1.97−1.91 (m, 6H), 1.68−1.58 (m, 6H), 1.44−1.23 (m, 54H), 0.97−0.84 (m, 45H) ^{13}C NMR (300 MHz, $CDCl_3$) δ (ppm): 161.85, 150.17, 149.04, 147.19, 144.24, 140.03, 139.64, 137.19, 130.84, 129.40, 128.73, 128.71, 128.56, 127.39, 126.21, 124.81, 124.17, 108.34, 108.18, 46.22, 39.50, 35.67, 33.68, 30.60, 28.82, 28.78, 23.94, 23.37, 22.58, 14.33, 14.18, 14.03, 10.86, 10.84, 10.71. Anal. Calcd for $C_{138}H_{165}N_7O_6S_6$: C, 74.99; H, 7.52; N, 4.44. Found: C, 74.81; H, 7.58; N, 4.47.

RESULTS AND DISCUSSION

Synthesis and Characterization of the Small Molecules. As shown in Scheme 1, the final products (P-DPP)$_3$TPA, (4-FP-DPP)$_3$TPA, and (4-BuP-DPP)$_3$TPA were synthesized by traditional palladium catalyzed Suzuki coupling of compound **4** with **3a**, **3b**, and **3c**, respectively. Compounds **1** and **4** were obtained by the reported procedures.[26] Compounds **2a**, **2b**, and **2c** were synthesized through Pd(0)-catalyzed Suzuki coupling of compound **1** with benzeneboronic acid, 4-fluoro-benzeneboronic acid, and 4-*n*-butyl-benzeneboronic acid, respectively. Compounds **3a**, **3b**, and **3c** were synthesized through simple bromination with *N*-bromosuccinimide (NBS). Three target molecules are all soluble in common organic solvents, such as CH_2Cl_2, $CHCl_3$, and toluene.

The thermal properties of these small molecules were investigated by thermogravimetric analyses (TGA), and the TGA curves were depicted in Figure 1. The small molecules,

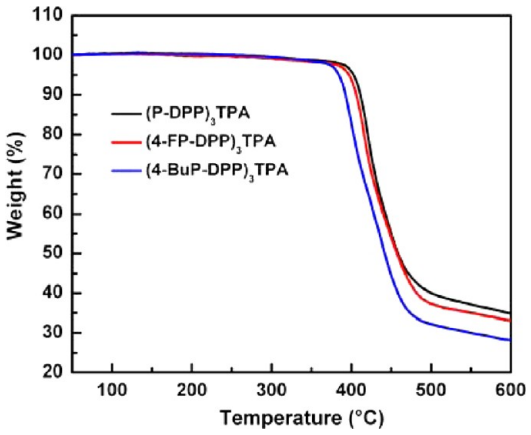

Figure 1. TGA curves of three small molecules.

(P-DPP)$_3$TPA, (4-FP-DPP)$_3$TPA, and (4-BuP-DPP)$_3$TPA all exhibit good thermal stability, with their 5% weight-loss temperatures (T_d) at 403, 396, and 383 °C under N_2 protection, respectively.

Optical Properties. The UV−visible absorption spectra of three small molecules in CH_2Cl_2 solutions and in thin films are shown in Figure 2. And the corresponding optical data are summarized in Table 1. In CH_2Cl_2 solution (Figure 2a), all three small molecules have two absorption peaks (λ_{max}) at 340 and 623 nm which can be assigned to the $\pi-\pi^*$ absorption of the molecule and ICT transition from electron-donating units (thiophene and TPA) to electron-accepting unit (DPP).[32−34] Moreover, from Figure 2a, it is shown that three molecules have the same absorption ranges, indicating the end groups have no obvious effect on molecular energy levels. Figure 3b shows the absorption spectra of the small molecules in thin films. Compared to the absorptions in dilute CH_2Cl_2 solution, there are the broadening of the absorption peaks and red shift of the absorption edge in films (for (P-DPP)$_3$TPA, 40 nm; (4-FP-DPP)$_3$TPA, 50 nm; and (4-BuP-DPP)$_3$TPA, 60 nm), which may be caused by the existence of $\pi-\pi$ stacking of the molecules in the dense states. As the absorption edges of the three small molecules are 720, 730, and 740 nm, the optical band gaps (E_g^{opt}) are calculated as 1.72, 1.70, and 1.68 eV for (P-DPP)$_3$TPA, (4-FP-DPP)$_3$TPA, and (4-BuP-DPP)$_3$TPA, respectively. Each small molecule exhibits a broad absorption range and a relatively low band gap, which would be in favor of light-harvesting when used as the active-layer material in OSCs. However, the absorption ranges of (P-DPP)$_3$TPA and (4-FP-DPP)$_3$TPA are broader than that of (4-BuP-DPP)$_3$TPA, which indicates that the size of the end groups have a dramatic influence on molecular packing and $\pi-\pi$ stacking in thin film. Larger end groups results in poorer molecular packing with narrower absorption range.

Electrochemical Properties. Figure 3 shows cyclic voltammograms (CV) of the three small molecules. And the electrochemical data are also summarized in Table 1. From Figure 3, all molecules exhibit quasi-reversible reduction/oxidation processes in the positive potential region. And each molecule has four reduction/oxidation couples which can be assigned to the successive oxidation of three arms and N atom in TPA core.

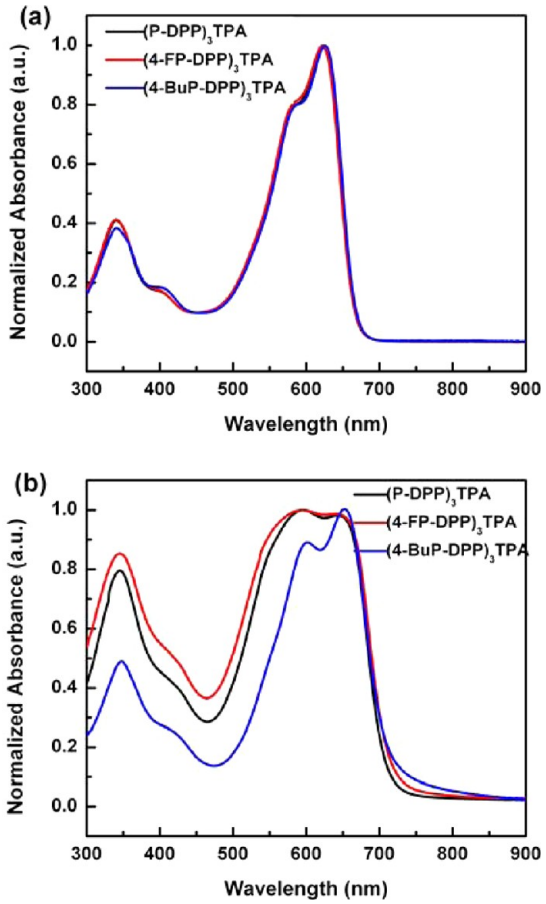

Figure 2. UV−vis absorption spectra of $(P\text{-}DPP)_3TPA$, $(4\text{-}FP\text{-}DPP)_3TPA$, and $(4\text{-}BuP\text{-}DPP)_3TPA$ in (a) CH_2Cl_2 solutions and (b) solid films.

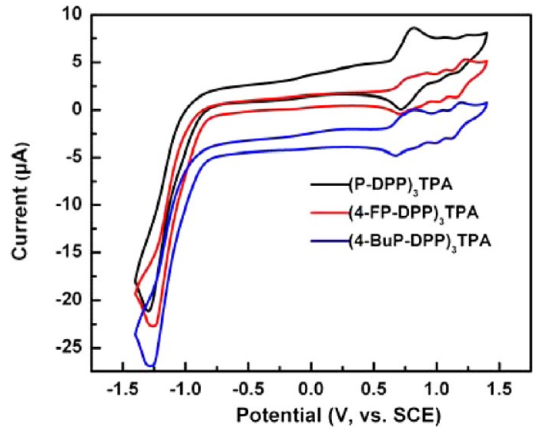

Figure 3. Cyclic voltammograms of $(P\text{-}DPP)_3TPA$, $(4\text{-}FP\text{-}DPP)_3TPA$, and $(4\text{-}BuP\text{-}DPP)_3TPA$ solutions in 0.1 mol/L Bu_4NPF_6 CH_2Cl_2 solution, at a scan rate of 50 mV/s.

However, no obvious redox waves are detected in the negative potential range, which indicates that all small molecules are typical p-type materials. HOMO values for all the materials were calculated from the corresponding oxidation onsets which were converted to SCE (saturated calomel electrode), based on −4.4 eV SCE energy level relative to vacuum using $E_{HOMO} = -(E_{ox} + 4.4)$ eV equation. From Table 1, the HOMO energy levels of $(P\text{-}DPP)_3TPA$, $(4\text{-}FP\text{-}DPP)_3TPA$ and $(4\text{-}BuP\text{-}DPP)_3TPA$ are −5.11, −5.13, and −5.09 eV, respectively. It is obvious that $(4\text{-}FP\text{-}DPP)_3TPA$ shows the lowest HOMO value (−5.13 eV) compared to the other two small molecules, indicating that the substitution of benzene ring with electron-withdrawing fluorine atom has effect on the decrease of the HOMO energy level.

Photovoltaic Properties. We explored the photovoltaic properties of the OSCs based on the three small molecules by fabricating BHJ devices with the structure of ITO/PEDOT:PSS/small molecule donor:$PC_{61}BM$/Al. Considering the effect of various solvents and blend ratios on the device performance,[23,34] the active layers were spin coated from different solvents (chlorobenzene and chloroform) using different weight ratio blends of small molecule donor:$PC_{61}BM$, respectively. And we found that chloroform is better than chlorobenzene. Furthermore, the effect of the additive (1,8-diiodooctane, DIO) on device performance was also investigated. The photovoltaic characteristics for different blend ratios are summarized in Table 2. From Table 2, it is found that the highest PCE of the device based on $(P\text{-}DPP)_3TPA$ is 2.98%, with a J_{sc} of 7.94 mA/cm^2, a V_{oc} of 0.72 V and a *FF* of 0.52. And, the $(4\text{-}FP\text{-}DPP)_3TPA$-based device exhibits a lower PCE of 1.63%, with a J_{sc} of 5.13 mA/cm^2, a V_{oc} of 0.76 V, and a *FF* of 0.42. $(4\text{-}BuP\text{-}DPP)_3TPA$-based device gives a PCE of 1.98% which is a bit higher than that of $(4\text{-}FP\text{-}DPP)_3TPA$, and the values of J_{sc}, V_{oc}, and *FF* are 5.83 mA/cm^2, 0.80 V and 0.42, respectively. Besides, the devices based on $(P\text{-}DPP)_3TPA$ and $(4\text{-}FP\text{-}DPP)_3TPA$ show better J_{sc} and PCE with decreasing donor concentration.

We attribute the difference in the OSC performances to the different charge transport properties and the different HOMO levels. Because the three arms of these molecules are not coplanar, molecular packing is disturbed. At low donor concentration (1:3 blend), the distance between adjacent molecules is beneficial for the molecular packing, resulting in enhanced charge transport. Although at higher donor concentration (1:1 blend), adjacent molecules are too close to form effective molecular packing, which may leads to poor J_{sc} and PCE. This hypothesis can be confirmed by AFM tests, and it will be discussed later.

From Table 2, the best photovoltaic devices of $(P\text{-}DPP)_3TPA$ and $(4\text{-}FP\text{-}DPP)_3TPA$ are obtained under the same condition. This can be attributed to the different steric hindrances in molecular packing. Because the end-group's size of $(4\text{-}BuP\text{-}DPP)_3TPA$ is the largest among three molecules, resulting in the poorest molecular packing. So the best device based on

Table 1. Optical and Electrochemical Properties of Three Small Molecules

small molecule	λ_{max} (nm) solution	λ_{onset} (nm) solution	λ_{max} (nm) film	λ_{onset} (nm) film	E_g^{opt}[a] (eV)	E_{ox}[b] (V)	HOMO[c] (eV)
$(P\text{-}DPP)_3TPA$	623	680	645	720	1.72	0.71	−5.11
$(4\text{-}FP\text{-}DPP)_3TPA$	623	680	647	730	1.70	0.73	−5.13
$(4\text{-}BuP\text{-}DPP)_3TPA$	623	680	653	740	1.68	0.69	−5.09

[a]Calculated from the absorption edges of the films, $E_g^{opt} = 1240/\lambda_{onset}$. [b]Onset potential of oxidation peaks versus SCE. [c]HOMO was obtained according to the empirical formulas HOMO = $-(E_{ox} + 4.4)$ eV.

dx.doi.org/10.1021/am302623k | ACS Appl. Mater. Interfaces 2013, 5, 972−980

Table 2. Photovoltaic Parameters of the Photovoltaic Devices under the Illumination of AM 1.5G Solar Irradiance (100 mW/cm^2)

donor material	blend ratio (D:$PC_{61}BM$)	solvent	μ_h (cm^2 (V s)$^{-1}$)	J_{SC} (mA/cm^2)	V_{oc} (V)	*FF*	PCE (%)
$(P\text{-}DPP)_3TPA$	1:1	$CHCl_3$		1.88	0.78	0.28	0.41
	1:2	$CHCl_3$		4.27	0.82	0.32	1.13
	1:3	$CHCl_3$		8.53	0.78	0.32	2.13
	1:1	$CHCl_3$+2% v/v DIO	$(8.63 \pm 0.98) \times 10^{-5}$	7.94	0.72	0.52	2.98
$(4\text{-}FP\text{-}DPP)_3TPA$	1:1	$CHCl_3$		1.58	0.74	0.32	0.28
	1:2	$CHCl_3$		4.21	0.82	0.35	1.19
	1:3	$CHCl_3$		4.70	0.84	0.38	1.51
	1:1	$CHCl_3$+2% v/v DIO	$(2.42 \pm 0.41) \times 10^{-5}$	5.14	0.76	0.42	1.63
$(4\text{-}BuP\text{-}DPP)_3TPA$	1:1	$CHCl_3$		2.08	0.80	0.28	0.47
	1:2	$CHCl_3$	$(4.43 \pm 0.22) \times 10^{-5}$	5.83	0.80	0.42	1.98
	1:3	$CHCl_3$		4.99	0.80	0.35	1.37
	1:1	$CHCl_3$+2% v/v DIO		2.27	0.76	0.54	0.31

$(4\text{-}BuP\text{-}DPP)_3TPA$ is gotten with lower donor concentration, which is different from the other two molecules. The *J*−*V* and EQE curves of the best photovoltaic devices are shown in Figures 4 and 5, respectively. And the relevant hole mobility of

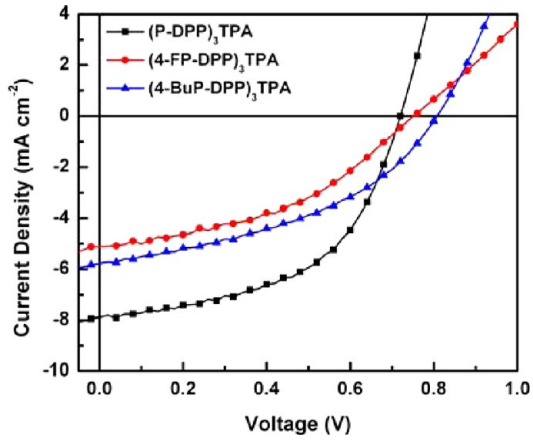

Figure 4. *J*−*V* characteristics of the best OSCs with small molecule donor:$PC_{61}BM$ blends as the active layers under illumination of AM 1.5G, 100 mW/cm^2.

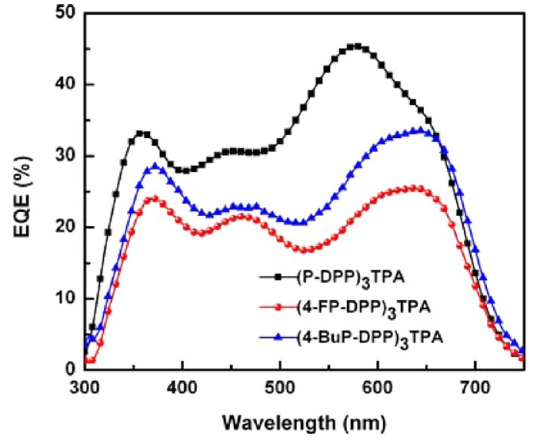

Figure 5. EQE curves of the best OSCs based on small molecule donor:$PC_{61}BM$ blends.

the blends was measured using the space-charge-limited current (SCLC) method, and *J*−*V* curves are shown in Figure 6. The highest PCE of $(P\text{-}DPP)_3TPA$ based device compared with the

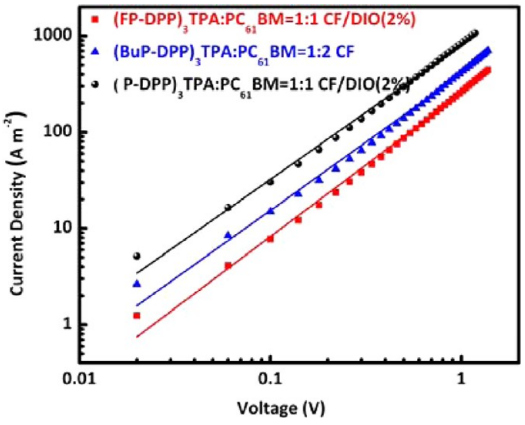

Figure 6. *J*−*V* characteristics of hole-only devices with a structure of ITO/PEDOT:PSS/small molecule donor:$PC_{61}BM$/MoO_3/Al. The symbols represent experimental data and the solid lines are fitted according to the Mott−Gurney Law.

other two small molecules based devices is probably due to the higher hole mobility ($(8.63 \pm 0.98) \times 10^{-5}$ cm^2 (V s)$^{-1}$). Possibly, in the star-shaped structure, end-capping groups (phenyl) without any substituent afford strong intermolecular orbital overlap and give a higher mobility and films processed with DIO can improve the morphology of $(P\text{-}DPP)_3TPA$:$PC_{61}BM$ blend, leading to a higher *FF*. $(4\text{-}FP\text{-}DPP)_3TPA$ based device has the highest V_{oc} of 0.84 V even though its PCE is the lowest among three small molecules based devices. This is due to the electron-withdrawing end-capping group (4-fluorophenyl). The result indicates that the introduction of fluorine (F) to the 4-position of phenyl group is beneficial for decreasing the HOMO energy of donor materials. Moreover, although the addition of DIO decreased the values of V_{oc}, it improved the values of J_{sc} and *FF* a lot. Maybe the addition of DIO forms efficient percolation channels for charge transport, which results in a higher J_{sc} and *FF*.

As shown in Figure 5, all devices show relatively high EQE in the range of 300−700 nm. Although the spectral ranges of these photovoltaic devices are almost equal, the maximum EQE value has reached 45.4% at 576 nm for the $(P\text{-}DPP)_3TPA$:$PC_{61}BM$ device. While the other two small molecules based devices show lower EQE values. So the device based on $(P\text{-}DPP)_3TPA$:$PC_{61}BM$ shows a higher J_{sc} than that of the other two molecule-based devices.

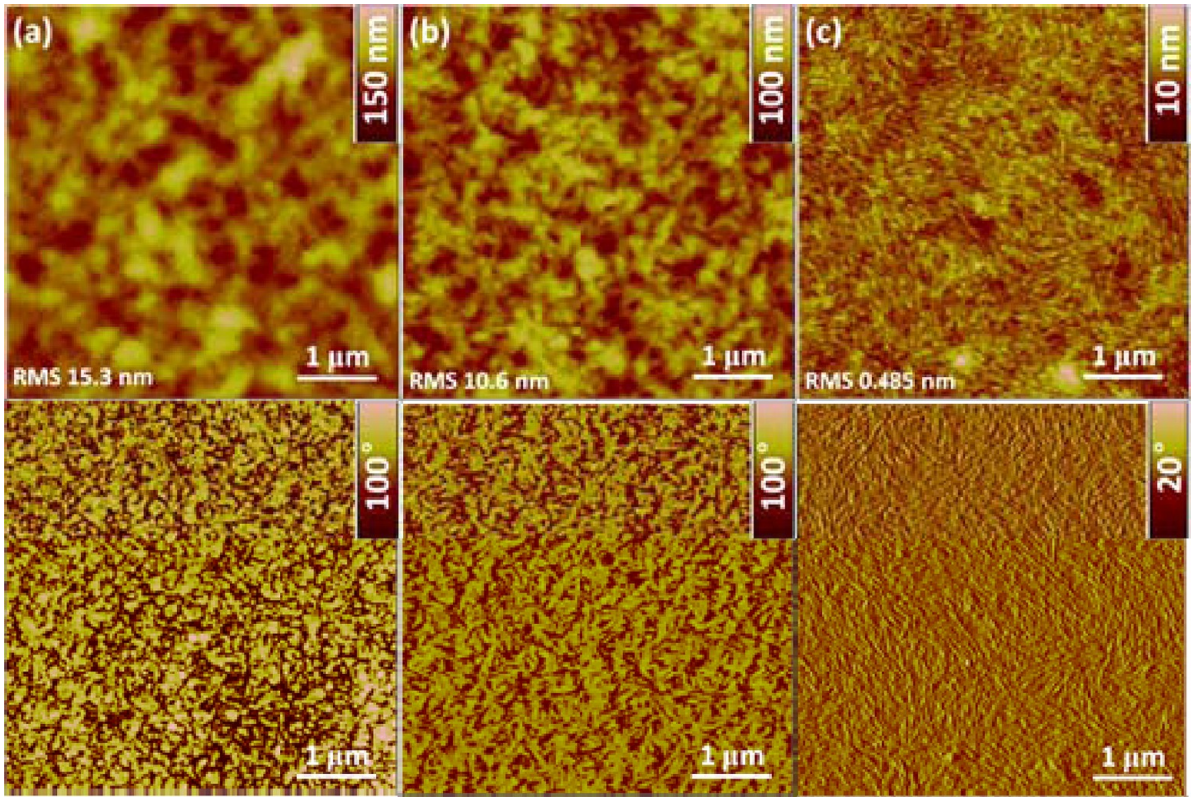

Figure 7. AFM images of donor molecule:$PC_{61}BM$ blended films showing the best photovoltaic performances. The upper and bottom are height and phase images, respectively. (a) $(P\text{-}DPP)_3TPA$:$PC_{61}BM$ film with 2% DIO; (b) $(4\text{-}FP\text{-}DPP)_3TPA$:$PC_{61}BM$ film with 2% DIO; (c) $(4\text{-}BuP\text{-}DPP)_3TPA$:$PC_{61}BM$ film. The scan size of the images is 5 μm × 5 μm.

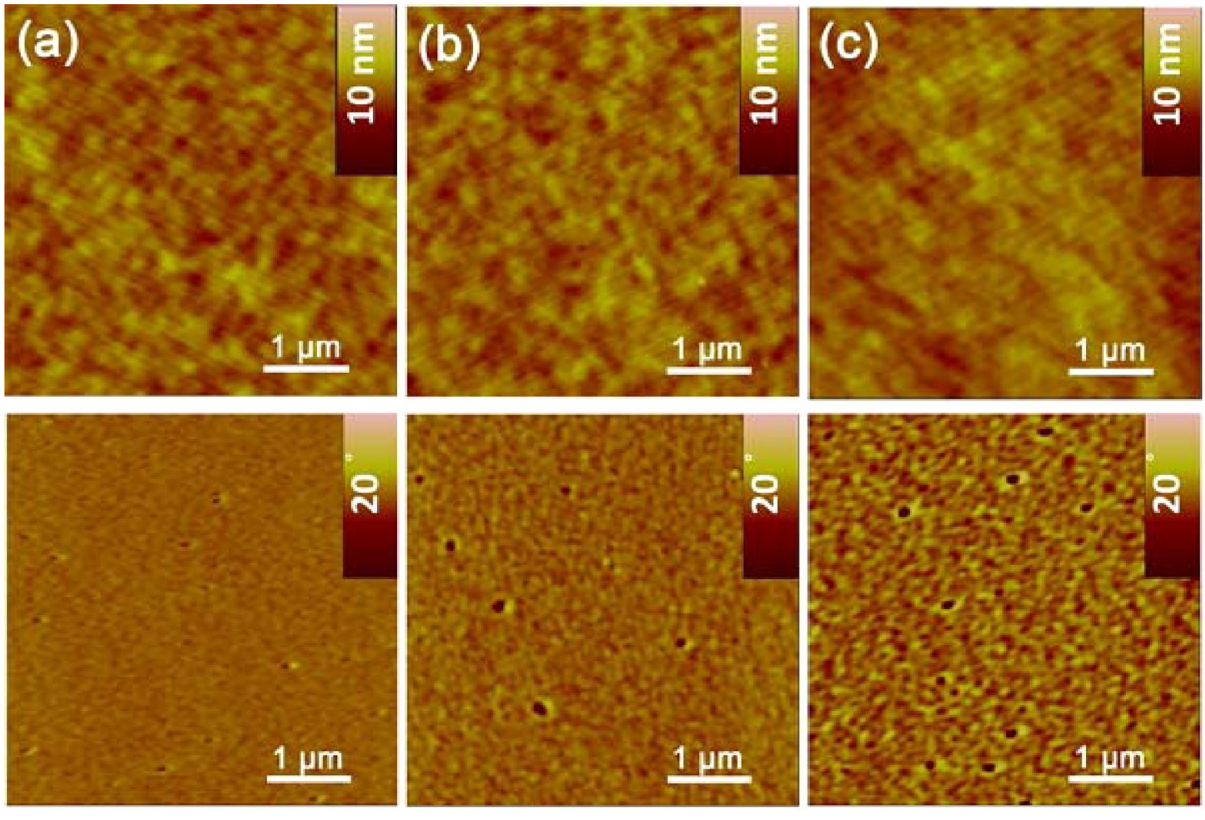

Figure 8. AFM images of $(P\text{-}DPP)_3TPA$:$PC_{61}BM$ films with different blend ratios. The upper and bottom are height and phase images, respectively. (a) $(P\text{-}DPP)_3TPA$:$PC_{61}BM$ = 1:1; (b) $(P\text{-}DPP)_3TPA$:$PC_{61}BM$ = 1:2; (c) $(P\text{-}DPP)_3TPA$:$PC_{61}BM$ = 1:3. The scan size of the images is 5 μm × 5 μm.

dx.doi.org/10.1021/am302623k | *ACS Appl. Mater. Interfaces* 2013, 5, 972−980

The morphology of the photoactive layer is very important for the photovoltaic performance of OSCs.[35,36] The morphology of small molecule:$PC_{61}BM$ blend films were investigated by atomic force microscopy (AFM). All blend films were prepared by spin-coating their $CHCl_3$ solution on the top of the PEDOT:PSS layer, which was spin-coated on the ITO glass. From Figure 7, it can be seen that the surface of $(4\text{-BuP-DPP})_3$-TPA:$PC_{61}BM$ blend is smoother than that of $(P\text{-DPP})_3TPA$ and $(4\text{-FP-DPP})_3TPA$-based blends, It is also shown that the addition of DIO makes the surfaces of blends rougher. Besides, the surface of $(4\text{-FP-DPP})_3TPA$:$PC_{61}BM$ blend is smoother than that of $(P\text{-DPP})_3TPA$-based blend even though they were investigated under the same condition. In general, the smoother morphology means finer D:A phase separation, which would lead to higher exciton dissociation efficiency. However, the device current correlates to the product of exciton dissociation and charge transport. Therefore, the highest J_{sc} of $(P\text{-DPP})_3TPA$-based device can be mainly ascribed to the most efficient charge transport among three molecules. As shown in AFM images of $(P\text{-DPP})_3TPA$:$PC_{61}BM$ films with different blend ratios (Figure 8), it is observed that, from Figure 8a–c, with the increase in $PC_{61}BM$ content, the contrast gradient increases, indicating that the degree of phase separation between $(P\text{-DPP})_3TPA$ and $PC_{61}BM$ increases, which may be beneficial to the exciton separation and charge transport. Thus the devices based on $(P\text{-DPP})_3TPA$ and $(4\text{-FP-DPP})_3TPA$ show better J_{sc} and PCE with the decreasing donor concentration.

CONCLUSION

In summary, a series of star-shaped D–A structure small molecules based on TPA and DPP with different end-capping groups have been designed and synthesized by Suzuki coupling reactions. All small molecules show a broad absorption range in visible region and good thermal stability. Optical band-gaps of these small molecules were calculated, ranging from 1.68 to 1.72 eV. Meanwhile, the photovoltaic devices based on these small molecules with $PC_{61}BM$ exhibit promising performance. The highest PCE of ~3% has been achieved for the devices using $(P\text{-DPP})_3TPA$ as donor with a J_{sc} of 7.94 mA/cm^2, a V_{oc} of 0.72 V and a *FF* of 0.52 processed from $CHCl_3$ under simulated AM 1.5G solar irradiation of 100 mW cm^{-2}.

AUTHOR INFORMATION

Corresponding Author

*Tel: +86-0571-87953733. E-mail: minminshi@zju.edu.cn.

Author Contributions

The manuscript was written through contributions of all authors. All authors have given approval to the final version of the manuscript.

Notes

The authors declare no competing financial interest.

ACKNOWLEDGMENTS

This work was supported by the National Natural Science Foundation of China (20774083, 50990063, 51073135) and Zhejiang Province Natural Science Foundation (Y407101). The work was also partly supported by Developing Program of Zhejiang Province Key Scientific and Technical Innovation Team (2009R50004) and the National High Technology Research and Development Program of China (863 Program) (2011AA050520).

REFERENCES

(1) Service, R. F. *Science* **2011**, *332*, 293–293.
(2) Walker, B.; Kim, C.; Nguyen, T. Q. *Chem. Mater.* **2011**, *23*, 470–482.
(3) Günes, S.; Neugebauer, H.; Sariciftci, N. S. *Chem. Rev.* **2007**, *107*, 1324–1338.
(4) Scharber, M. C.; Mühlbacher, D.; Koppe, M.; Denk, P.; Waldauf, C.; Heeger, A. J.; Brabec, C. J. *Adv. Mater.* **2006**, *18*, 789–794.
(5) Li, X. H.; Choy, W. C. H.; Huo, L. J.; Xie, F. X.; Sha, W. E. I.; Ding, B. F.; Guo, X.; Li, Y. F.; Hou, J. H.; You, J. B.; Yang, Y. *Adv. Mater.* **2012**, *24*, 3046–3052.
(6) Hu, X. L.; Shi, M. M.; Chen, J.; Zuo, L. J.; Fu, L.; Liu, Y. J.; Chen, H. Z. *Macromol. Rapid Commun.* **2011**, *32*, 506–511.
(7) Shi, M. M.; Deng, D.; Chen, L.; Ling, J.; Fu, L.; Hu, X. L.; Chen, H. Z. *J. Polym. Sci., Part A: Polym. Chem.* **2011**, *49*, 1453–1461.
(8) Huan, Y.; Guo, X.; Liu, F.; Huo, L. J.; Chen, Y. N.; Russell, P. R.; Han, C. C.; Li, Y. F.; Hou, J. H. *Adv. Mater.* **2012**, *24*, 3383–3389.
(9) He, Z. C.; Zhong, C. M.; Su, S. J.; Xu, M.; Wu, H. B.; Cao, Y. *Nat. Photonics* **2012**, *6*, 591–595.
(10) Zhou, J. Y.; Wan, X. J.; Liu, Y. S.; Zuo, Y.; Li, Z.; He, G. R.; Long, G. K.; Ni, W.; Li, C. X.; Su, X. C.; Chen, Y. S. *J. Am. Chem. Soc.* **2012**, *134*, 16345–16351.
(11) Loser, S.; Bruns, C. J.; Miyauchi, H.; Ortiz, R. P.; Facchetti, A.; Stupp, S. I.; Marks, T. J. *J. Am. Chem. Soc.* **2011**, *133*, 8142–8145.
(12) van der Poll, T. S.; Love, J. A.; Nguyen, T. Q.; Bazan, G. C. *Adv. Mater.* **2012**, *24*, 3646–3649.
(13) Dutta, P.; Yang, W.; Eom, S. H.; Lee, S. H. *Org. Electron.* **2012**, *13*, 273–282.
(14) Zhang, J.; Yang, Y.; He, C.; Deng, D.; Li, Z. B.; Li, Y. F. *J. Phys. D: Appl. Phys.* **2011**, *44*, 475101.
(15) Yang, Y.; Zhang, J.; Zhou, Y.; Zhao, G. J.; He, C.; Li, Y. F.; Andersson, M.; Inganäs, O.; Zhang, F. L. *J. Phys. Chem. C* **2010**, *114*, 3701–3706.
(16) Shang, H. X.; Fan, H. J.; Liu, Y.; Hu, W. P.; Li, Y. F.; Zhan, X. W. *Adv. Mater.* **2011**, *23*, 1554–1557.
(17) Shi, Q. Q.; Cheng, P.; Li, Y. F.; Zhan, X. W. *Adv. Energy Mater.* **2012**, *2*, 63–67.
(18) Cho, N.; Kim, J.; Song, K.; Lee, J. K.; Ko, J. *Tetrahedron* **2012**, *68*, 4029–4036.
(19) Hu, X. L.; Zuo, L. J.; Fu, W. F.; Larsen-Olsen, T. T.; Helgesen, M.; Bundgaard, E.; Hagemann, O.; Shi, M. M.; Krebs, F. C.; Chen, H. Z. *J. Mater. Chem.* **2012**, *22*, 15710–15716.
(20) Qu, S.; Tian, H. *Chem. Commun.* **2012**, *48*, 3039–3051.
(21) Sharma, G. D.; Mikroyannidis, J. A.; Sharma, S. S.; Roy, M. S.; Thomas, K. R. J. *Org. Electron.* **2012**, *13*, 652–666.
(22) Chen, M. R.; Fu, W. F.; Shi, M. M.; Hu, X. L.; Pan, J. Y.; Ling, J.; Li, H. Y.; Chen, H. Z. *J. Mater. Chem. A* **2013**, *1*, 105–111.
(23) Huo, L. J.; Hou, J. H.; Chen, H. Y.; Zhang, S. Q.; Jiang, Y.; Chen, T. L.; Yang, Y. *Macromolecules* **2009**, *42*, 6564–6571.
(24) Walker, B.; Tomayo, A. B.; Dang, X. D.; Zalar, P.; Seo, J. H.; Garcia, A.; Tantiwiwat, M.; Nguyen, T. Q. *Adv. Funct. Mater.* **2009**, *19*, 3063–3069.
(25) Lin, Y. Z.; Cheng, P.; Li, Y. F.; Zhan, X. W. *Chem. Commun.* **2012**, *48*, 4773–4775.
(26) Sahu, D.; Tsai, C. H.; Wei, H. Y.; Ho, K. C.; Chang, F. C.; Chu, C. W. *J. Mater. Chem.* **2012**, *22*, 7945–7953.
(27) Huo, L. J.; Zhang, S. Q.; Guo, X.; Xu, F.; Li, Y. F.; Hou, J. H. *Angew. Chem., Int. Ed.* **2011**, *50*, 9697–9702.
(28) Bijleveld, J. C.; Gevaerts, V. S.; Di NUZZO, D.; Turbiez, M.; Mathijssen, S. G. J.; de LeeUw, D. M.; Wienk, M. M.; Janssen, R. A. J. *Adv. Mater.* **2010**, *22*, E242–E246.
(29) Dutta, P.; Yang, W.; Eom, S. H.; Lee, W. H.; Kang, I. N.; Lee, S. H. *Chem. Commun.* **2012**, *48*, 573–575.
(30) Yasuda, T.; Shinohara, Y.; Matsuda, T.; Han, L.; Ishi-i, T. *J. Mater. Chem.* **2012**, *22*, 2539–2544.

(31) Kylberg, W.; Sonar, P.; Heier, J.; Tisserant, J. -N.; Müller, C.; Nüesch, F.; Chen, Z. −K.; Dodabalapur, A.; Yoon, S.; Hany, R. *Energy Environ. Sci.* **2011**, *4*, 3617−3624.
(32) Ripaud, E.; Olivier, Y.; Leriche, P.; Cornil, J.; Roncali, J. *J. Phys. Chem. B* **2011**, *115*, 9379−9386.
(33) Lee, S. K.; Cho, J. M.; Goo, Y.; Shin, W. S.; Lee, J. C.; Lee, W. H.; Kang, I. N.; Shim, H. K.; Moon, S. J. *Chem. Commun.* **2011**, *47*, 1791−1793.
(34) Wienk, M. M.; Turbiez, M.; Gilot, J.; Janssen, R. A. J. *Adv. Mater.* **2008**, *20*, 2556−2560.
(35) Ma, W. L.; Yang, C. Y.; Gong, X.; Lee, K.; Heeger, A. J. *Adv. Funct. Mater.* **2005**, *15*, 1617−1622.
(36) Li, G.; Shrotriya, V.; Huang, J. S.; Yao, Y.; Moriarty, T.; Emery, K.; Yang, Y. *Nat. Mater.* **2005**, *4*, 864−868.